Chinese Society of Aeronautics and Astronautics
& Beihang University

Chinese Journal of Aeronautics

cja@buaa.edu.cn
www.sciencedirect.com

Numerical simulation of RCS for carrier electronic warfare airplanes

CrossMark

Yue Kuizhi [a,b], **Liu Wenlin** [a], **Li Guanxiong** [b], **Ji Jinzu** [b,*], **Yu Dazhao** [a]

[a] *Department of Airborne Vehicle Engineering, Naval Aeronautical and Astronautical University, Yantai 264001, China*
[b] *School of Aeronautic Science and Engineering, Beihang University, Beijing 100191, China*

Abstract This paper studies the radar cross section (RCS) of carrier electronic warfare airplanes. Under the typical naval operations section, the mathematical model of the radar wave's pitch angle incidence range analysis is established. Based on the CATIA software, considering dynamic deflections of duck wing leading edge flaps, flaperons, horizontal tail, and rudder, as well as aircraft with air-to-air missile, anti-radiation missile, electronic jamming pod, and other weapons, the 3D models of carrier electronic warfare airplanes Model *A* and Model *B* with weapons were established. Based on the physical optics method and the equivalent electromagnetic flow method, by the use of the RCSAnsys software, the characteristics of carrier electronic warfare airplanes' RCS under steady and dynamic flights were simulated under the UHF, X, and S radar bands. This paper researches the detection probability of aircraft by radars under the condition of electronic warfare, and completes the mathematical statistical analysis of the simulation results. The results show that: The Model *A* of carrier electronic warfare airplane is better than Model *B* on stealth performance and on discover probability by radar detection effectively.

1. Introduction

Carrier electronic warfare airplane is one of the necessary models on modern aircraft carriers, where carrier electronic warfare airplanes, strike fighters, early warning aircraft, helicopters, and transport aircraft unite the carrier aircraft wing together. The EA-6B carrier-borne aircraft of the United States is a carrier electronic warfare aircraft on active service on the Nimitz-class aircraft carriers. It was modified and researched on the basis of the A-6 carrier strike aircraft. The EA-18G carrier-borne aircraft is the next generation of carrier electronic warfare airplane in the United States, which was modified and researched on the basis of the F/A-18F carrier strike aircraft. The derivative of the U.S. carrier electronic warfare aircraft is of great reference for the aircraft configuration of Chinese carrier aircraft wing.

The characteristics of the radar cross section (RCS) of carrier electronic warfare airplanes are not only the performance which aircraft design and manufacturing units are concerned, but also one of the performance indicators that the military

ELSEVIER **Production and hosting by Elsevier**

is concerned when used in combat. The military armaments department puts forward the stealth performance indicators of carrier electronic warfare airplanes, expecting to reduce the aircraft's RCS characteristics. At the same time, the army's combat troops analyze the RCS characteristics of carrier electronic warfare airplanes under the conditions of different pitching angles and azimuth angles based on active service aircraft, expecting to win local wars under high-tech conditions based on current equipment. At present, many scholars' researches of electronic warfare and stealth characteristics of aircraft are deeper. In the field of electronic warfare, scholars studied the gray characteristics of test management of electronic warfare systems,[1] analyzed the electronic interference power assignment method in cooperative air combats of mixed formation,[2] discussed the dynamic decision making method for cooperation of airborne hard kill/soft kill weapons,[3] and analyzed cooperative generation of phantom radar track using a team of electronic combat air vehicles based on range gate pull-off.[4] In the field of aircraft conceptual design and stealth design, scholars at home and abroad studied radar stealth, infrared stealth, visible light stealth, and acoustic stealth technologies, as well as the aerodynamic configuration stealth of the fuselage and the wing, air inlet stealth, surface crack stealth, and other key technologies of the shape-stealth. They also discussed the material stealth technology and summarized the avionics/RF system and other solutions of the radar stealth technology.[5] Some other scholars studied the RCS model and algorithm and other related contents. For example, Li et al.[6] studied Gaussian beam on the terahertz radar cross section of a conducting cylinder distribution. Shi et al.[7] studied RCS statistical characterization using Weibull distribution. Li et al.[8] established a comprehensive stealth performance analysis method and evaluated stealth aircraft based on the RCS characteristics of different targets. Wu and Gong[9] studied methods of reducing the RCS of a radar antenna. Chung[10] completed the numerical simulation of RCS of a metal cone and a plasma covered metal cone. These researches have reference values for the numerical simulation of a 3D digital model's RCS. Liu et al.[11] three new control factors were proposed to calculate a multilevel fast multiple algorithm, and the calculation efficiency was improved. Huang et al.[12] studied recognition of the major scattering sources on complex targets based on the high frequency RCS integrated calculation technique, which is suitable for solving large complex targets and targets that need a lower RCS accuracy. Ledger and Morgan[13] established a reduced-order model. A 3D electromagnetic scattering numerical simulation was made in the paper, and it could forecast monostatic RCS quickly. Park and Kim[14] put forward an angular division algorithm, which accelerated the prediction of RCS values for large and complex objective models. Although experts and scholars made a lot of contribution in the field of electronic warfare and aircraft stealth in the past, there are shortages of researches in the two fields. Academic papers about carrier electronic warfare airplanes have not been collected. Researches about the influence of an incident wave's pitching angle on RCS characteristics are not in place under operational conditions, and researches of the range of the wave's pitching angle are not concrete at the time of stealth design. Researches on RCS characteristics of aircraft and the detection probability of aircraft under the condition of electronic interference are not thorough.

Based on previous studies, from analyzing the pitching angle of radar incident wave in the operational profile of a carrier electronic warfare airplane, this paper established the 3D computer aided three-dimensional interface application (CATIA) models of carrier electronic warfare airplanes. Based on the physical optics method and the equivalent electromagnetic flow method, by the use of developed RCSAnsys software, the RCS characteristics of carrier electronic warfare airplanes were analyzed. This paper also researched the detection probability of aircraft by radars of different wave bands under the condition of electronic interference. This paper expected to provide technical supports for RCS characteristics of carrier electronic warfare airplane research, and to put forward a reference of the strategy to reduce RCS of carrier electronic warfare airplanes.

2. Theoretical basis

The theoretical basis of numerical simulation of a carrier electronic warfare airplane's RCS characteristics includes the following three aspects: the analysis of the pitching angle of radar incident wave in the operational profile, the RCS calculation method, and the detection probability model in the condition of electronic warfare.

2.1. Analysis of the pitching angle of radar incident wave in the operational profile

In modern air and sea battles, a carrier electronic warfare airplane faces threats of radar and other electronic equipment on the enemy's aircraft carriers, destroyers, carrier-based strike fighters, and electronic warfare and early warning airplanes. After analyzing the American 3D defense system of the aircraft carrier battle group, this paper concluded the schematic diagram of the pitching angle of radar incident wave in the operational profile in Fig. 1.

Fig. 1 illustrates that the pitching angle of the enemy's radar incident wave related to the aircraft under the typical operational profile is as follows:

$$\beta = \beta_f - \frac{180}{\pi} \arcsin \frac{h_d - h_m}{l} \tag{1}$$

$$l \leqslant \left\{ \sqrt{(h_m + R_d)^2 - R_d^2} + \sqrt{(h_d + R_d)^2 - R_d^2} \right\} \tag{2}$$

where β is the pitching angle of the incident wave relative to the aircraft, which is negative when the radar incident wave is under the aircraft, β_f the pitching angle of the shipboard electronic warfare aircraft relative to the ground, and β_f
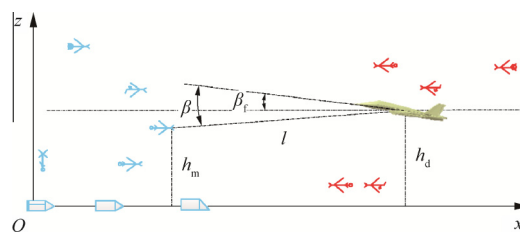

Fig. 1   Pitching angle of radar incident wave.

negative when the nose is upward, h_d the distance between the aircraft and the sea level, h_m the distance between the target equipment and the sea level, l the distance between the detection radar of the target equipment and the carrier electronic warfare airplane; R_d the radius of the earth, which is 6371 km in general.

Eq. (2) is the constraint condition of Eq. (1). Radar wave cannot illuminate to the aircraft when Eq. (2) is not set up. In the derivation process of Eq. (1), because the radius of the earth is close to infinity compared with the flight height of the aircraft, the influence of the radius of the earth to the aircraft pitching angle relative to the incident wave is ignored.

2.2. RCS calculation method

In this paper, the physical optics method and the equivalent electromagnetic flow method are used to numerically simulate the RCS characteristics of the carrier electronic warfare airplane.

The equation used by the physical optics method to calculate surface scattering is as follows:

$$\sqrt{\sigma_{po}} = -j \frac{k}{\sqrt{\pi}} \int_s \hat{\boldsymbol{n}} \cdot (\hat{\boldsymbol{e}}_r \times \hat{\boldsymbol{h}}_i) \exp[jk\boldsymbol{r} \bullet (\hat{\boldsymbol{i}} - \hat{\boldsymbol{s}})] \mathrm{d}S \quad (3)$$

where $\sqrt{\sigma_{po}}$ is the RCS of one surface, j the imaginary unit and $j^2 = -1$. $k = 2\pi/\lambda$ the free space wave number, λ the radar incident wavelength, $\hat{\boldsymbol{n}}$ the unit vector of outer normal direction of the surface, $\hat{\boldsymbol{e}}_r$ the unit vector of electric field direction of the receiving antenna, $\hat{\boldsymbol{h}}_i$ the unit vector of magnetic field direction of the incident wave, $\bullet$ the dot product, $\times$ the cross product, $\boldsymbol{r}$ the vector of the local origin to the surface of unit $\mathrm{d}S$, $\hat{\boldsymbol{i}}$ the unit vector of incidence direction, $\hat{\boldsymbol{s}}$ the unit vector of scattering direction, $\hat{\boldsymbol{s}} = \frac{\boldsymbol{s}}{|\boldsymbol{s}|}$, $\boldsymbol{s}$ is the scattering direction.

The equation of the equivalent electromagnetic flow method is

$$\sqrt{\sigma_{ecm}} = \frac{1}{\sqrt{\pi} \sin \theta} \Big[(\boldsymbol{E}_0^i \bullet \boldsymbol{t}) f \boldsymbol{s} \times (\boldsymbol{s} \times \boldsymbol{t}) \\ - Z_0 (\boldsymbol{H}_0^i \bullet \boldsymbol{t}) g \boldsymbol{s} \times \boldsymbol{t} \Big] \cdot e^{-j2k\boldsymbol{r}_t \cdot \boldsymbol{s}} \frac{\sin(k\boldsymbol{l} \bullet \boldsymbol{s})}{k\boldsymbol{l} \bullet \boldsymbol{s}} \quad (4)$$

where $\boldsymbol{t}$ is the mandatory edge unit vector direction, θ the included angle of incidence directions $\boldsymbol{i}$ and $\boldsymbol{t}$, $\boldsymbol{E}_0^i$ the strength of the incident electric field, f and g are the Yoffie Rousseff diffraction coefficient, Z_0 the wave impedance in vacuum, $\boldsymbol{H}_0^i$ the strength of the incident magnetic field, $\boldsymbol{r}_t$ the position vector of the middle of the edge; l the vector of the edge.[15–19]

The superposition equations of the aircraft are as follows:

$$\sigma = \left| \sum_{i=1}^n (\sqrt{\sigma_{po}})_i + \sum_{i=1}^n (\sqrt{\sigma_{ecm}})_i \right|^2 \quad (5)$$

The arithmetic mean value equation of RCS is as follows:

$$\bar{\sigma}_{n\sim N}^\beta = \frac{1}{N-n+1} \sum_{\varphi=n}^N \sigma_\varphi^\beta \quad (6)$$

The unit conversion equation is as follows:

$$\sigma_{dBm^2} = 10 \lg \sigma \quad (7)$$

where σ_φ^β is the RCS value where the incoming wave pitch angle is β and the azimuth angle is φ, $\bar{\sigma}_{n\sim N}^\beta$ the arithmetic mean value where the incoming wave pitch angle is β and the

azimuth angle is φ ($\varphi = n\sim N$), σ the RCS of the aircraft, $\bar{\sigma}$ the arithmetic mean value of the aircraft's RCS, σ_{dBm^2} the RCS of the aircraft.

2.3. Detection probability model in the condition of electronic warfare

The probability of finding a target while the radar is searching is

$$P_D = \exp \left(-\frac{9.5\sqrt{\Omega}}{\sqrt{\Delta\theta_\alpha f_r S_{jk}}} \right) \quad (8)$$

When there is no interference, in Eq. (8):

$$S_{jk} = \frac{P_t G^2 \lambda^2 E \bar{\sigma}_\beta^{\pm 15°}}{(4\pi)^3 k_b T_0 B_n F_n L R^4} \quad (9)$$

When there is interference, in Eq. (8):

$$S_{jk} = \frac{P_t G_t \Delta f_j \bar{\sigma}_\beta^{\pm 15°}}{P_j G_j v_j \Delta f_r 4\pi R^2} \quad (10)$$

where P_D is the probability of finding a target, Ω the angular scanning speed, $\Delta\theta_\alpha$ the horizontal beamwidth; f_r the repetition frequency, S_{jk} the signal to noise ratio of the individual pulse, P_t the power of transmitter, G the antenna gain, λ the radar wavelength, E the pulse compression ratio, $\bar{\sigma}_\beta^{\pm 15°}$ the arithmetic mean value of the aircraft when the forward azimuth angles are $\pm 15°$ and the pitching angle is β, k_b Boltzmann's constant, T_0 the standard room temperature, B_n the noise bandwidth, F_n the noise factor, L the total loss of system, R the distance between the enemy radar and the carrier electronic warfare airplane, G_t the radar transmitting antenna gain, Δf_j the receiver jamming signal bandwidth, P_j the power of jammer, G_j the antenna gain of jammer, v_j the polarization loss of the jamming signal, Δf_r the receiver bandwidth.[20]

After mastering these theories, the RCS characteristics of the carrier electronic warfare airplane can be analyzed.

3. Electromagnetic test validation method

This paper studied the RCS characteristics of the carrier electronic warfare airplane. Based on the physical optics method and the equivalent electromagnetic flow method, this paper completed the digital simulation of the RCS characteristics of the aircraft by the use of the RCSAnsys software. RCSAnsys is a kind of software which tests and analyzes characteristics of an aircraft's RCS. It was developed based on the numerical analysis of an aircraft's RCS. Before analyzing an aircraft's RCS characteristics, the scientificity and accuracy of the calculation method of RCSAnsys should be tested by the electromagnetic test.

3.1. Electromagnetic test verification of aircraft RCS numerical simulation

In this paper, CATIA software is used to create the 3D digital aircraft models in Fig. 2. Then, the digital aircraft models are imported to the RCSAnsys software to numerically simulate the aircraft's RCS and conclude the curve of the aircraft's RCS characteristics.
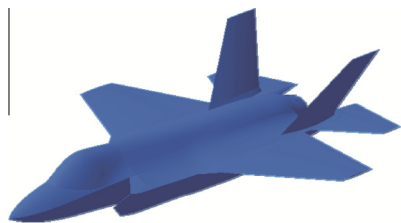
Fig. 2 3D digital models of the aircraft.

In this paper, a 3D printer is used to create the 3D scale entity model of the aircraft as shown in Fig. 3(a). Then, the model is electromagnetically tested in an anechoic chamber as shown in Fig. 3(b). Finally, the aircraft RCS characteristic curve of the electromagnetic test is obtained after conversion as shown in Fig. 4.

3.2. Conclusion of electromagnetic test

In this section, based on the physical optics method and the equivalent electromagnetic flow method, the RCSAnsys software is used to simulate the RCS characteristics of the 3D digital aircraft model, and after that, compare the result with the RCS characteristics obtained from the electromagnetic test. The result is shown in Fig. 4. The initial conditions of the numerical simulation and experiment are: the incident wave of radar is X band, the radar incident wavelength is 3 cm, the pitching angle of the incident wave is 0°, the polarization method is horizontal, and the azimuth angle of the plane is 0–180°. It is concluded from Fig. 4 that the RCS value from the numerical simulation is in line with that from the electromagnetic test. The conclusion proves that the method is scientific and the numerical simulation is accurate. Next, the software is used to simulate the RCS characteristics of the carrier electronic warfare airplane.
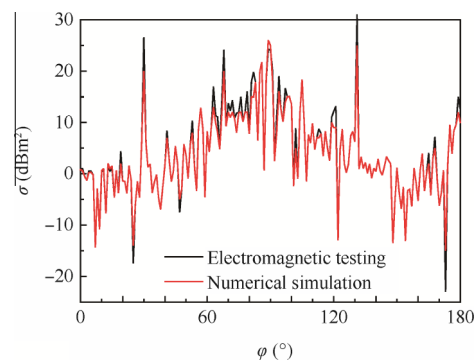

(a) Entity model of aircraft
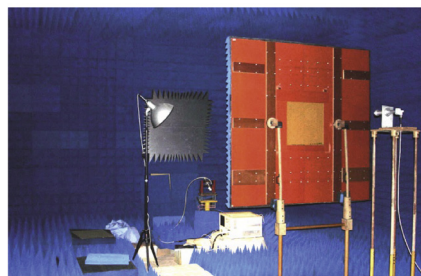
(b) Anechoic chamber

Fig. 3 Electromagnetic test of aircraft in an anechoic chamber.

Fig. 4 RCS characteristics from numerical simulation and electromagnetic test.

4. Aircraft RCS characteristics simulation and analysis

Aircraft RCS characteristics simulation and analysis include the following 5 steps:

Step 1. 3D digital model establishing of the carrier electronic warfare airplane.
Step 2. Radar incident wave pitching angle analysis in the aircraft operational profile.
Step 3. Aircraft RCS simulation and analysis.
Step 4. RCS characteristics analysis of the carrier-borne electronic warfare aircraft in climb and dive.
Step 5. Detection probability of aircraft analysis.

4.1. 3D digital model establishing of the carrier electronic warfare airplane

In this paper, CATIA software is used to establish the 3D digital model of the carrier electronic warfare airplane. 3D digital model establishing of the carrier electronic warfare airplane includes the following 3 sections: 3D models of the aircraft; 3D models of electronic warfare equipment and weapons; 3D models of the electronic warfare airplane.

4.1.1. 3D models of aircraft

In this section, on the background of the EA-18G carrier electronic warfare airplane in the U.S. and the carrier electronic warfare airplane derived from the Su-33 carrier-based aircraft in Russia, CATIA software is used to establish the 3D digital model as shown in Fig. 5. Because EA-18G and Su-33 do not use stealth-absorbing materials, the RCS characteristics of the two aircraft are mainly dependent on the shape of the plane. The 3D models are simplified under the condition that the main RCS characteristics can be expressed. The basic size data of two carrier electronic warfare airplanes are in Table 1.

In Fig. 5, Model *A* carrier electronic warfare airplane is a kind of normal aerodynamic configuration aircraft with a two-seater, a twin-engine, twin extraversion vertical tails, a stabilator, and a large strake wing. This aircraft has leading edge flaps and flaperons on wings. Model *B* carrier electronic warfare airplane is a kind of tri-surface aerodynamic configuration aircraft with a two-seater, a twin-engine, twin vertical tails, a stabilator, and a large strake wing. This aircraft also has leading edge flaps and flaperons on wings.

(a) Model A   (b) Model B

Fig. 5   3D aircraft digital models.

Table 1   Basic size data of two carrier electronic warfare airplanes.

Data	Model A	Model B
Length (m)	18.31	21.18
Span (m)	11.43	14.7
Height (m)	4.66	5.72

4.1.2. 3D models of electronic warfare equipment and weapons

Because the carrier electronic warfare airplane is usually equipped with soft- and hard-killing weapons, this section presents 3D digital models of air-to-air missiles, anti-radiation missiles, and electronic jamming pods as shown in Fig. 6.

4.1.3. 3D models of electronic warfare airplanes

The carrier airplane will become a carrier electronic warfare airplane after being equipped with electronic warfare equipment and weapons and fitment modifying. The geometric model of the carrier electronic warfare airplane is based on the normal aircraft, and 2 air-to-air missiles, 2 anti-radiation missiles, and 5 electronic jamming pods are added.

    After establishing 3D CATIA models of carrier electronic warfare airplanes, the analysis of the radar incident wave pitching angle in operational profile and the RCS characteristics numerical simulation can be done.

4.2. Analysis of radar incident wave pitching angle in operational profile

In this section, the relation of the radar incident wave pitching angle with the distance is obtained as shown in Fig. 7 based on Eqs. (1) and (2), and the initial condition is $\beta_f = -3°$.

    In Fig. 7, the horizontal axis represents the distance from the detection radar of a target to the carrier electronic warfare airplane. The vertical axis represents the pitching angle of the radar incident wave to the airframe.

    Fig. 7(a) shows the relation of the radar incident wave pitching angle β with l under conditions that the height of the carrier electronic warfare airplane above the sea level is $h_d = 5.0$ km, the flight height of the carrier early warning plane is $h_m = 8.00$ km, the fight heights of the carrier strike fighters are $h_m = 4.00$ km and 1 km, and the height of aircraft-warning radars on aircraft carriers and destroyers is $h_m = 0.05$ km.
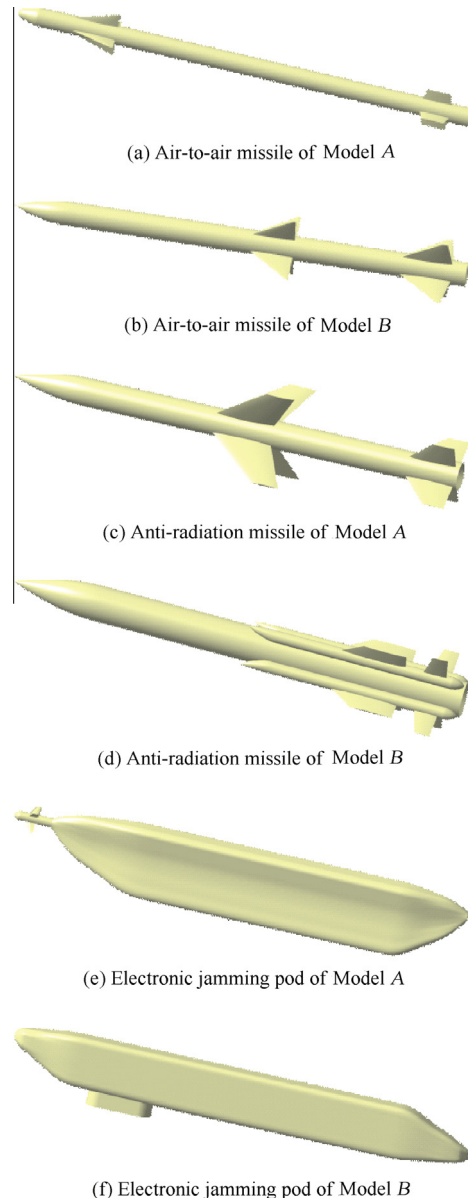

(a) Air-to-air missile of Model A

(b) Air-to-air missile of Model B

(c) Anti-radiation missile of Model A

(d) Anti-radiation missile of Model B

(e) Electronic jamming pod of Model A

(f) Electronic jamming pod of Model B

Fig. 6   3D digital models of electronic warfare equipment and weapons.

Under above conditions, it is known from Fig. 7(a) that: the maximum distance of the carrier early warning plane to detect the carrier electronic warfare airplane is 571 km, the
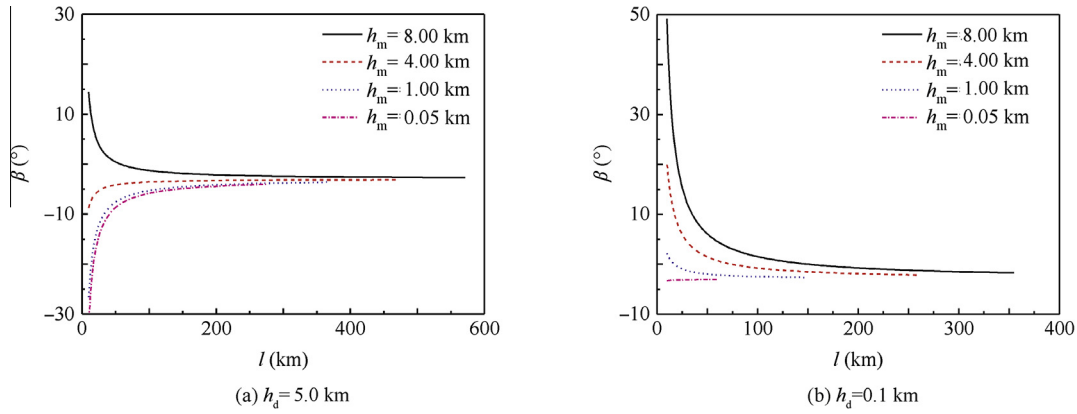
(a) $h_d = 5.0$ km

(b) $h_d = 0.1$ km

Fig. 7 Radar incident wave pitching angle variation.

radar incident wave pitching angle β is $-2.69°$ at the moment, and β is $3.89°$ when the detection distance is 25 km; the maximum distance of the carrier strike fighter to detect the carrier electronic warfare airplane is 478 km when the height of the carrier strike fighter is $h_m = 4.00$ km, β is $-3.11°$ at the moment, and β is $-5.29°$ when the detection distance is 25 km; the maximum distance of the carrier strike fighter to detect the carrier electronic warfare airplane is 356 km when the height of the carrier strike fighter is $h_m = 1.00$ km, β is $-3.62°$ at the moment, and β is $-12.20°$ when the detection distance is 25 km; the maximum distance of aircraft-warning radars on aircraft carriers and destroyers to detect the carrier electronic warfare airplane is 277 km, β is $-4.02°$ at the moment, and β is $-14.42°$ when the detection distance is 25 km. It can be seen that when the level flight height of the carrier electronic warfare airplane is 5 km, the incident wave pitching angle of radars outside 25 km and under the height of 8 km is within the range of $-14.42°$ to $3.89°$.

In a similar way, when the carrier electronic warfare airplane flies levelly, and the flight height is 0.1 km, Fig. 7(b) shows that the maximum distance of the carrier early warning plane which flies at the height of 8 km to detect the carrier electronic warfare airplane is 355 km; the maximum distance of the carrier strike fighter which flies at the height of 4 km to detect the carrier electronic warfare airplane is 261 km, and the distance is 148 km when the flight height of the carrier strike fighter is 1 km; the maximum distance of 0.05 km high aircraft-warning radars on aircraft carriers and destroyers to detect the carrier electronic warfare airplane is 60 km. The incident wave pitching angle of radars outside 25 km and under the height of 8 km is within the range of $-3.11°$ to 15.42°.

The following conclusion can be drawn: while designing the stealth plane of which flight height is within the range of 0.1 km–5 km, the detection distance of radars outside 25 km and under the height of 8 km can be reduced if reducing the RCS of the plane of which the pitching angle β is between $-14.42°$ and 15.42°. On the other hand, while performing the radar detection numerical simulation of planes of which the level flight height is within the range of 0.1 km–5.0 km, only the RCS of planes of which the pitching angle β is between $-14.42°$ and 15.42° need to be analyzed, and then all the detection distances of radars outside 25 km and under the height of 8 km can be satisfied.

### 4.3. Aircraft RCS numerical simulation and analysis

In naval warfare, carrier electronic warfare airplanes mainly face the detections of UHF band early warning radars on early warning planes, X band fire control radars on strike fighters, and S band aircraft-warning radars on aircraft carriers and destroyers. Under the condition of the same pitching angles and azimuth angles of the radar incident wave, and under the detections of UHF, X, S, and other different bands radars, the RCS values of the same carrier electronic warfare airplane are different.

In this section, based on Eqs. (3)–(5), and referring to the typical radar incident wave pitching angle and radar bands concluded in Section 4.2, the RCSAnsys software is used to simulate the RCS of the 3D digital aircraft models built in Section 4.1, and then the intensity distribution of the RCS of the carrier electronic warfare airplane is obtained as shown in Figs. 8 and 9 under the condition of horizontal polarization, and the RCS characteristics as shown in Fig. 10(a) and (b) are obtained at the same time.
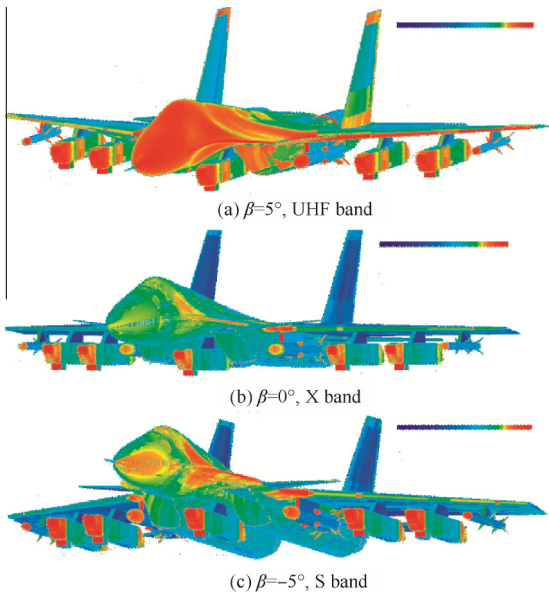
Fig. 8(a) is the RCS intensity distribution of Model A carrier electronic warfare airplane obtained by simulation, which is under the condition that the radar on the carrier early warning plane is UHF band, the pitching angle of incident wave is $\beta = 5°$, and the azimuth angle of the plane is 16°; Fig. 8(b) is the RCS intensity distribution of Model A under the condition that the fire control radar on the carrier strike fighter is X band, $\beta = 0°$, and the azimuth angle of the plane is 16°; Fig. 8(c) is the RCS intensity distribution of Model A under the condition that the aircraft-warning radars on aircraft carriers and destroyers are S band, $\beta = -5°$, and the azimuth angle of the plane is 16°.

It is known from Fig. 8(a) that aiming at the detection of UHF band radar on the carrier early warning plane, the carrier electronic warfare airplane needs to reduce the RCS of the radome, canopy, upper surface of the strake wing, and other parts. It also needs to be covered with camouflage coating aiming at the UHF band and contour stealthy design of the nose.

It is known from Fig. 8(b) that aiming at the detection of X band fire control radar on the carrier strike fighter, the carrier electronic warfare airplane needs to reduce the RCS of the radome, canopy, strake wings, air inlets, air-to-air missiles, anti-radiation missiles, electronic jamming pods, and other parts. It also needs to be covered with camouflage coating

(a) β=5°, UHF band

(b) β=0°, X band

(c) β=−5°, S band
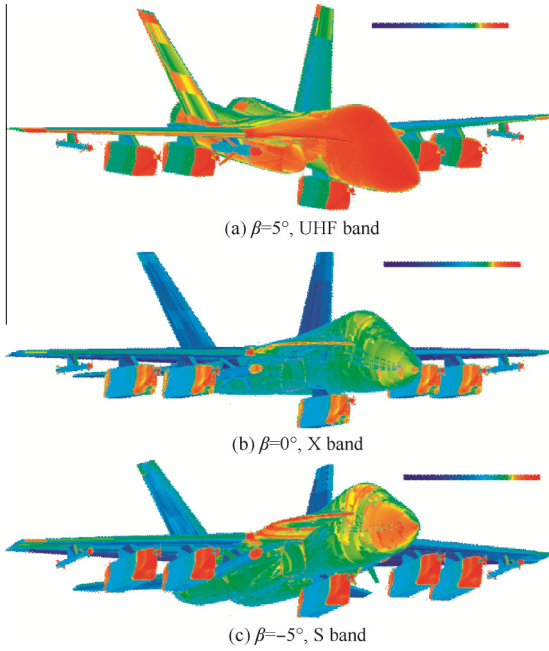
Fig. 8 RCS intensity distribution of Model A carrier electronic warfare airplane under the condition of variable pitching angles (azimuth angle is 16°).

(a) β=5°, UHF band

(b) β=0°, X band

(c) β=−5°, S band

Fig. 9 RCS intensity distribution of Model B carrier electronic warfare airplane under the condition of variable pitching angles (azimuth angle is 344°).

aiming at the X band and contour stealthy designs of the nose and air inlets.

It is known from Fig. 8(c) that aiming at the detection of S band aircraft-warning radars on aircraft carriers and destroyers, the carrier electronic warfare airplane needs to reduce the RCS of the air inlets, mounted weapons, and other parts. It also needs to be covered with camouflage coating aiming at

the S band and contour stealthy designs of the nose and air inlets.

Fig. 9(a) is the RCS intensity distribution of Model B carrier electronic warfare airplane obtained by simulation, which is under the condition that the radar on the carrier early warning plane is UHF band, the pitching angle of incident wave is $\beta = 5°$, and the azimuth angle of the plane is 344°; Fig. 9(b) is the RCS intensity distribution under the condition that the fire control radar on the carrier strike fighter is X band, $\beta = 0°$, and the azimuth angle of the plane is 344°; Fig. 9(c) is the RCS intensity distribution under the condition that the aircraft-warning radars on aircraft carriers and destroyers are S band, $\beta = -5°$, and the azimuth angle of the plane is 0°.

In a similar way, it is known from Fig. 9 that aiming at the detection of UHF, X, and S band radars, the carrier electronic warfare airplane needs to reduce the RCS of the radome, canopy, strake wings, air inlets, air-to-air missiles, anti-radiation missiles, electronic jamming pods, and other parts. It also needs to be covered with camouflage coating and contour stealthy designs of the nose and air inlets.

By conversions of Eqs. (6) and (7), it is obtained from Fig. 10(a) that under the condition of UHF band and $\beta = 5°$, the $\pm 15°$ head-on RCS arithmetic mean value $\bar{\sigma}_{6°}^{\pm 15°}$ of Model A carrier electronic warfare airplane is -1.53 dBm^2, the $\pm 15°$ lateral RCS arithmetic mean value $\bar{\sigma}_{6°}^{\pm 15°}$ is 20.64 dBm^2, and the $\pm 15°$ backward RCS arithmetic mean value $\bar{\sigma}_{6°}^{\pm 15°}$ is 2.97 dBm^2. It is obtained from Fig. 10(a) that under the condition of X band and $\beta = 0°$, the $\pm 15°$ head-on RCS arithmetic mean value $\bar{\sigma}_{0°}^{\pm 15°}$ of Model A carrier electronic warfare airplane is 3.43 dBm^2, the lateral $\bar{\sigma}_{0°}^{\pm 15°}$ is 22.46 dBm^2, and the backward $\bar{\sigma}_{0°}^{\pm 15°}$ is 12.19 dBm^2. It is obtained from Fig. 10(a) that under the condition of S band and $\beta = -5°$, the head-on $\bar{\sigma}_{-3°}^{\pm 15°}$ of Model A carrier electronic warfare airplane is 9.69 dBm^2, the lateral $\bar{\sigma}_{-3°}^{\pm 15°}$ is 20.79 dBm^2, and the backward $\bar{\sigma}_{-3°}^{\pm 15°}$ is 3.99 dBm^2.

It is obtained from Fig. 10(b) that under the condition of UHF band and $\beta = 5°$, the $\pm 15°$ head-on RCS arithmetic mean value $\bar{\sigma}_{6°}^{\pm 15°}$ of Model B carrier electronic warfare airplane is 0.37 dBm^2, the $\pm 15°$ lateral RCS arithmetic mean value $\bar{\sigma}_{6°}^{\pm 15°}$ is 21.55 dBm^2, and the $\pm 15°$ backward RCS arithmetic mean value $\bar{\sigma}_{6°}^{\pm 15°}$ is 1.45 dBm^2. It is obtained from Fig. 10(b) that under the condition of X band and $\beta = 0°$, the $\pm 15°$ head-on RCS arithmetic mean value $\bar{\sigma}_{0°}^{\pm 15°}$ of Model B carrier electronic warfare airplane is 4.73 dBm^2, the lateral $\bar{\sigma}_{0°}^{\pm 15°}$ is 37.44 dBm^2, and the backward $\bar{\sigma}_{0°}^{\pm 15°}$ is 13.02 dBm^2. It is obtained from Fig. 10(b) that under the condition of S band and $\beta = -5°$, the head-on $\bar{\sigma}_{-3°}^{\pm 15°}$ of Model B carrier electronic warfare airplane is 6.90 dBm^2, the lateral $\bar{\sigma}_{-3°}^{\pm 15°}$ is 21.09 dBm^2, and the backward $\bar{\sigma}_{-3°}^{\pm 15°}$ is 7.47 dBm^2.

It is known from data comparison of Fig. 10(a) and (b) that comparing the RCS characteristics of Model A with those of Model B, the conclusions are as follows:

(1) Under the UHF band, the head-on $\bar{\sigma}_{6°}^{\pm 15°}$ is reduced by 34.73%, the lateral $\bar{\sigma}_{6°}^{\pm 15°}$ is reduced by 18.76%, and the backward $\bar{\sigma}_{6°}^{\pm 15°}$ is increased by 41.69%.
(2) Under the X band, the head-on $\bar{\sigma}_{0°}^{\pm 15°}$ is reduced by 25.81%, the lateral $\bar{\sigma}_{0°}^{\pm 15°}$ is reduced by 96.82%, and the backward $\bar{\sigma}_{0°}^{\pm 15°}$ is reduced by 17.23%.

(a) Model *A*   (b) Model *B*

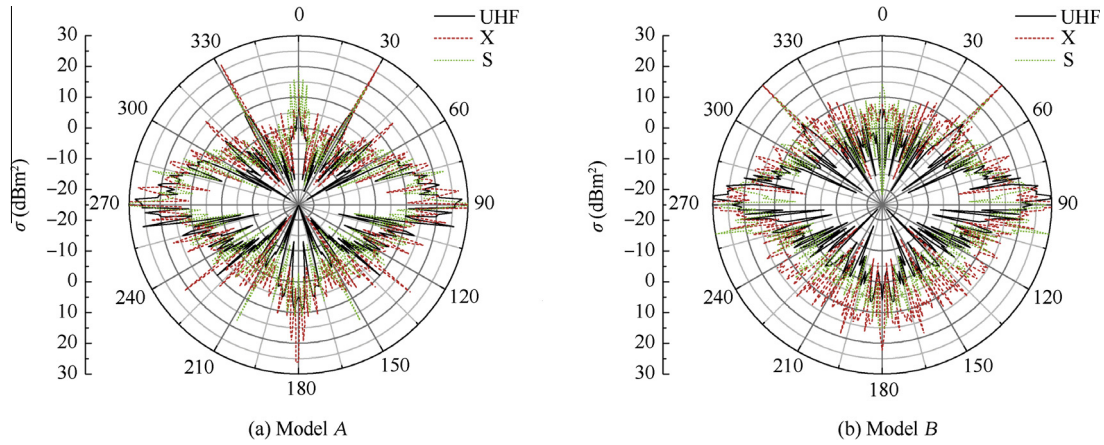**Fig. 10**   RCS characteristics of Model *A* carrier electronic warfare airplane.

(3) Under the S band, the head-on $\bar{\sigma}_{-3°}^{\pm15°}$ is increased by 90.41%, the lateral $\bar{\sigma}_{-3°}^{\pm15°}$ is reduced by 6.66%, and the backward $\bar{\sigma}_{-3°}^{\pm15°}$ is reduced by 55.11%.

The reasons that the RCS of Model *A* is reduced compared with that of Model *B* are as follows:

(1) The size of Model *A* is smaller than that of Model *B*. The length of Model *A* is reduced by 13.55%, the span by 22.24%, and the height by 18.53% (The basic size is in Table 1).
(2) Model *A* uses twin extraversion vertical tails while Model *B* uses twin vertical tails, so the lateral RCS of Model *A* is reduced a lot.
(3) Through simulating the RCS characteristics of the two 3D models, we know the RCS of Model *A*'s electronic jamming pod is smaller than that of Model *B*'s.

4.4. RCS characteristics analysis of carrier-borne electronic warfare aircraft in climb and dive

This paper analyses not only the RCS characteristics of the carrier-borne electronic warfare aircraft in balanced flight, but also the RCS characteristics in mobile processes, such as climb and dive. This section analyses the RCS characteristics of the aircraft during climbing and diving, including three links: the establishment of the geometric model, the numerical simulation of the RCS, and the mathematical statistics analysis of the RCS.

(1) The establishment of the geometric model

Duck wing, frontal flap, flaperon, horizontal tail, and other rudder surfaces will be deflected when the carrier-borne electronic warfare aircraft is in subduction and climb.

When climbing, the rudder surface deflection angle of Model *A* plane is set as follows: the front flap deflects down 5°, the flaperon deflects down 25°, and the horizontal tail deflects down 25°.

When diving, the rudder surface deflection angle of Model *A* plane is set as follows: the front flap deflects 0°, the flaperon deflects 0°, and the horizontal tail deflects up 25°.

When climbing, the rudder surface deflection angle of Model *B* plane is set as follows: the duck wing deflects up 10°, the front flap deflects down 5°, the flaperon deflects down 25°, and the horizontal tail deflects down 25°.

When diving, the rudder surface deflection angle of Model *B* plane is set as follows: the duck wing deflects down 10°, the front flap deflects down 0°, the flaperon deflects down 0°, and the horizontal tail deflects up 25°.

(2) Numerical simulation of airplanes' RCS

When the incident wave of the radar is X band and horizontal polarization, and under the condition that the pitching angle of the incident wave is −5°, 0°, and 5°, based on the physical optics method and the equivalent electromagnetic flow method, the RCS characteristics of Model *A* and Model *B* carrier-borne electronic warfare aircraft in climbing and diving have been calculated, as shown in Fig. 11.

(3) RCS contrastive analysis

The mathematical statistics of the RCS characteristics of the aircraft in Fig. 11 have been done, and contrastive analysis is shown in Table 2.

It's known from Fig. 10(a) and (b), and Table 2 that the RCS characteristics in climbing and diving are very different from those in balanced flight. Therefore, this paper suggests: when a plane is approaching enemy targets, before the plane has been found, the pilot should make the plane in balanced flight and avoid doing big maneuvering flight, in order to avoid enemy radar, for the airplane's RCS fluctuation is too large.

4.5. Detection probability analysis of carrier electronic warfare airplane

After obtaining the RCS characteristics curves of the aircraft, this paper anglicized the detection probability of the carrier electronic warfare airplane under the conditions with and without electronic jamming.

The detection probability of the aircraft is obtained by numerical simulation based on Eqs. (8)–(10) as shown in Fig. 12(a) and (b). Initial conditions of numerical simulation are as follows: the power of transmitter P_t is 10 MW; the
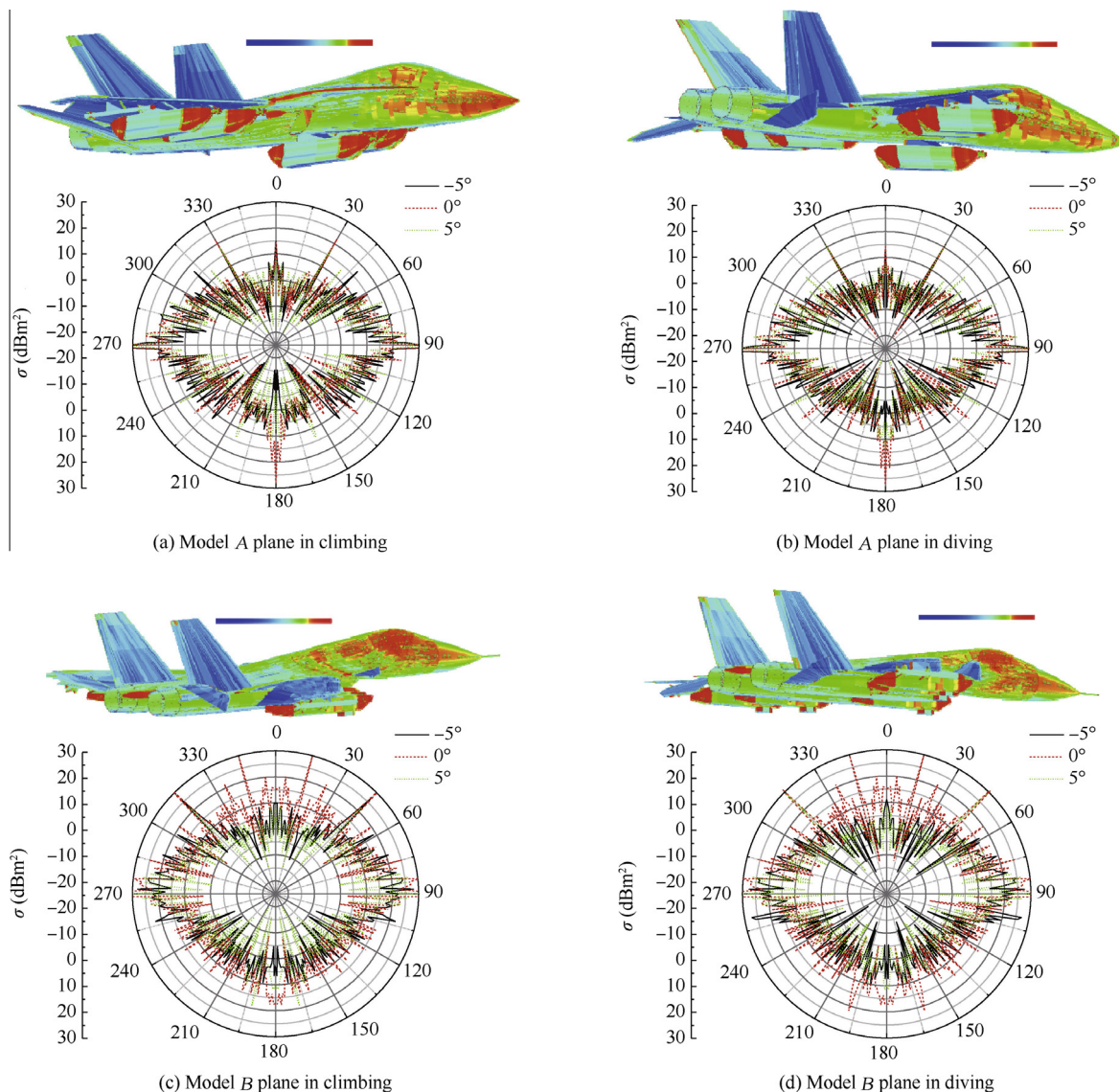
(a) Model A plane in climbing

(b) Model A plane in diving

(c) Model B plane in climbing

(d) Model B plane in diving

Fig. 11 RCS characteristics of carrier-borne electronic warfare aircraft when climbing and diving.
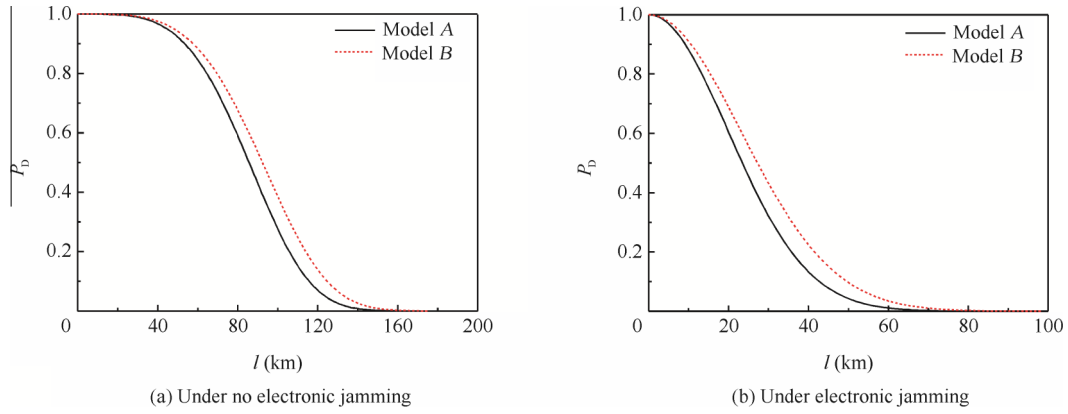
Table 2 Mathematical statistics of RCS characteristics in climbing and diving.

Mobile process	Pitching angle of incident wave	RCS mean value of Model A in $\pm 30°$(dBm^2)			RCS mean value of Model B in $\pm 30°$(dBm^2)		
		Head-on	Lateral	Backward	Head-on	Lateral	Backward
Climbing	$-5°$	5.736	19.794	2.543	4.158	17.958	5.016
Climbing	$0°$	8.514	21.476	14.430	16.998	30.704	11.787
Climbing	$5°$	5.555	18.558	5.782	1.983	18.484	8.027
Diving	$-5°$	7.652	19.788	2.348	3.305	18.525	4.600
Diving	$0°$	7.170	21.734	14.554	17.008	30.873	13.201
Diving	$5°$	7.356	18.216	4.586	1.909	18.677	4.648

antenna gain G is 100 dB; the pulse compression ratio E is 300; Boltzmann's constant k is 1.38×10^{-23} W·s/K; the standard room temperature T_0 is 290 K; the power of jammer P_j is 20 kW; the polarization loss of the jamming signal v_j is 0.5; the total loss of system L is 20 dB; the noise bandwidth B_n is 0.077 MHz; the noise factor F_n is 55 dB; the horizontal beamwidth $\Delta\theta_\alpha$ is 7°; the repetition frequency f_r is 300 Hz; the angular scanning speed Ω is 30(°)/s; the antenna gain of

jammer G_j is 7 dB; the receiver bandwidth Δf_r is 1.44 MHz; the receiver jamming signal bandwidth Δf_j is 1.44 MHz; the radar transmitting antenna gain G_t is 36 dB; the flight heights of Model A and Model B are 5 km; the radar wavelength $\lambda = 0.03$ m.

When the radar is X band, the RCS of Model A is $\bar{\sigma}_{0°}^{\pm 15°} = 3.43$ dBm^2 = 2.20 m^2, and the RCS of Model B is $\bar{\sigma}_{0°}^{\pm 15°} = 4.73$ dBm^2 = 2.97 m^2.

(a) Under no electronic jamming   (b) Under electronic jamming

Fig. 12 Detection probability of the carrier electronic warfare airplane.

Fig. 12(a) describes the detection probability of the carrier electronic warfare airplane under no electronic jamming, and Fig. 12(b) describes the detection probability under electronic jamming. In both figures, the horizontal axis represents the distance between the radar and the carrier electronic warfare airplane, and the vertical axis represents the detection probability of the aircraft by radar.

It is known from Fig. 12(a) that when there is no electronic jamming, under the condition that the detection probability is 5%, the distance between Model A carrier electronic warfare airplane and the carrier strike fighter using X band radar is 123 km, and the distance between Model B and the carrier strike fighter is 134 km. Compared with the detection distance of Model B, the distance of Model A is reduced by 8.20%.

It is known from Fig. 12(b) that when there is electronic jamming, under the condition that the detection probability is 5%, the distance between Model A carrier electronic warfare airplane and the carrier strike fighter using X band radar is 48 km, and the distance between Model B and the carrier strike fighter is 56 km. Compared with the detection distance of Model B, the distance of Model A is reduced by 14.28%.

It is known from Fig. 12(a) and (b) that when the radar band is X, the detection distance of Model A under electronic jamming is reduced by 60.97% compared with the distance under no electronic jamming. Similarly, when the radar band is X, the detection distance of Model B under electronic jamming is reduced by 58.20% compared with the distance under no electronic jamming.

In the detection probability numerical simulation and analysis, the reason why Model A is better than Model B is that the RCS of Model A is smaller than that of Model B. So in order to reduce the RCS of Model B, stealth modifications need to be done on Model B.

5. Conclusions

In this paper, the RCS characteristics of the EA-18G carrier electronic warfare airplanes and electronic warfare airplane derived from Su-33 have been analyzed. Based on CATIA software, under the condition of different deflections of control surfaces and mounting missiles and electronic jamming pods, the 3D model of carrier electronic warfare airplanes under dynamic flight has been built in this paper. Based on the physical optics method and the equivalent electromagnetic flow method, under different bands of radar, the RCS characteristics of two carrier electronic warfare airplanes under smooth flight and dynamic flight have been simulated in this paper, and the detection probability of aircraft by radars has also been researched. Then, a RCS reduction strategy of carrier electronic warfare airplanes in stealth subsequent modification has been put forward. Through research in this paper, the conclusions are as follows:

(1) While designing stealth planes of which the level flight height is within the range of 0.1–5.0 km, only the RCS of planes of which the pitching angle β is between $-14.42°$ and $15.42°$ need to be analyzed, and then all the detection distances of radars outside 25 km and under the height of 8 km can be satisfied.

(2) Aiming at the detection of UHF, X, and S bands radars, the carrier electronic warfare airplane needs to reduce the RCS of the radome, canopy, strake wings, air inlets, vertical tails, air-to-air missiles, anti-radiation missiles, electronic jamming pods, and other parts. It also needs to be covered with camouflage coating and contour stealthy designs of the nose and air inlets.

(3) Comparing the RCS characteristics of Model A with those of Model B, the conclusions are as follows.

a) Under the UHF band, the head-on $\bar{\sigma}_{6°}^{\pm15°}$ is reduced by 34.73%, the lateral $\bar{\sigma}_{6°}^{15°}$ is reduced by 18.76%, and the backward $\bar{\sigma}_{6°}^{\pm15°}$ is increased by 41.69%.

b) Under the X band, the head-on $\bar{\sigma}_{0°}^{\pm15°}$ is reduced by 25.81%, the lateral $\bar{\sigma}_{0°}^{15°}$ is reduced by 96.82%, and the backward $\bar{\sigma}_{0°}^{15°}$ is reduced by 17.23%.

c) Under the S band, the head-on $\bar{\sigma}_{-3°}^{\pm15°}$ is increased by 90.41%, the lateral $\bar{\sigma}_{-3°}^{\pm15°}$ is reduced by 6.66%, and the backward $\bar{\sigma}_{-3°}^{15°}$ is reduced by 55.11%.

(4) When the plane is approaching enemy targets, before the plane has been found, the pilot should make the plane in balanced flight and avoid doing big maneuvering flight, in order to avoid enemy radar, for the airplane's RCS fluctuation is too large.

(5) When the radar band is X, the detection distance of Model A under electronic jamming is reduced by 60.97% compared with the distance under no electronic jamming. The detection distance of Model B under electronic jamming is reduced by 58.20% compared with the distance under no electronic jamming.

(6) In order to reduce the RCS of Model *B*, stealth modifications need to be done on Model *B*.

Research conclusions of this paper are expected to provide technical support for scattering characteristics research of carrier electronic warfare airplanes and to provide references for stealth research of carrier electronic warfare airplanes.

Acknowledgement

References

1. Ke HF, Chen YG, Liu SF. Research on grey characteristics of test management of electronic warfare system and its application. *Acta Armamentarll* 2009;**30**(5):592–6.
2. Fu ZW, Yu L, Kou YX. Electronic jamming power assignment method in cooperative air combat of mixed formation. *Syst Eng Electron* 2012;**34**(6):1171–5 [Chinese].
3. Wang YH, Gao XG, Fan H. Dynamic decision making method for cooperation of airborne hardkill/softkill weapons. *Syst Eng Electron* 2012;**34**(9):1822–8 [Chinese].
4. Gao B, Mao SY. Cooperative generation of phantom radar track using a team of ECAVS based on RGPO. *J Beijing Univ Aeronaut Astronaut* 2011;**37**(11):1343–6 [Chinese].
5. Sun C, Zhang P. Lo requirements and solutions of avionics/RF system for advanced aircraft. *Acta Aeronaut Astronaut Sin* 2008;**29**(6):1472–81 [Chinese].
6. Li HY, Li Q, Xue K, Zhao YP. Research into influence of gaussian beam on terahertz radar cross section of a conducting cylinder distribution. *J Infrared Millimeter Terahertz Waves* 2013;**34**(3):289–98.
7. Shi WQ, Shi XW, Xu L. Radar cross section (RCS) statistical characterization using Weibull distribution. *Microwave Opt Technol Lett* 2013;**55**(6):1355–8.
8. Li Y, Huang J, Hong S. A new assessment method for the comprehensive stealth performance of penetration aircrafts. *Aerosp Sci Technol* 2011;**15**(7):511–8.
9. Wu T, Li Y, Gong SX. A novel low RCS microstrip antenna using aperture coupled microstrip dipoles. *J Electromagn Waves Appl* 2008;**22**(7):953–63.
10. Chung SSM. FDTD simulations on radar cross sections of metal cone and plasma covered metal cone. *Vacuum* 2011;**86**(7):970–84.
11. Liu ZH, Huang PL, Gao X. Multi-frequency RCS reduction characteristics of shape stealth with MLFMA with improved MMN. *Chin J Aeronaut* 2010;**23**(3):327–33.
12. Huang MJ, Lyu MY, Huang J. Recognition of the major scattering sources on complex targets based on the high frequency radar cross section integrated calculation technique. *J Shanghai Univ* 2009;**13**(4):115–21.
13. Ledger PD, Morgan K. An adjoint enhanced reduced-order model for monostatic RCS computation. *Electromagnetics* 2008;**28**(1–2):54–76.
14. Park KK, Kim HT. RCS prediction acceleration and reduction of table size for the angular division algorithm. *J Electromagn Waves Appl* 2009;**23**(11–12):1657–64.
15. Yue KZ, Sun C, Ji JZ. Numerical simulation on the stealth characteristics of twin-vertical-tails for fighter. *J Beijing Univ Aeronaut Astronaut* 2014;**40**(2):160–5 [Chinese].
16. Yue KZ, Sun C, Liu H, Su M. Numerical simulation on the RCS of combat aircraft for mounted missile. *Syst Eng Electron* 2014;**36**(1):62–7 [Chinese].
17. Yue KZ, Tian YF, Liu H, Han W. Conceptual design and RCS property research of three-surface strike fighter. *Int J Aeronaut Space Sci* 2014;**15**(3):309–19.
18. Ruan YZ. *Radar cross section and stealth technology*. Beijing: National Defense Industry Press; 1998. p. 99–120 [Chinese].
19. Baussard A, Rochdi M, Khenchaf A. PO/MEC-based bistatic scattering model for complex objects over a sea surface. *Prog Electromagn Res* 2011;**111**(1):229–51.
20. Yue KZ, Hou ZQ, Yang YK. Markov model of efficiency of volleying anti-ship missiles piercing into ship-bone antiaircraft missiles. *J Syst Simul* 2010;**22**(6):1472–5 [Chinese].

Yue Kuizhi is currently pursuing his Ph.D. degree in the School of Aeronautic Science and Engineering at Beihang University. His research interests mainly include aircraft conceptual design, aircraft stealth, and carrier aircraft security.

Liu Wenlin received his Ph.D. degree at Naval Aeronautical and Astronautical University in 2006. His research interests mainly include aircraft conceptual design, unmanned aerial vehicles, and aircraft security.

Li Guanxiong is currently pursuing his Ph.D. degree in the School of Aeronautic Science and Engineering at Beihang University. His research interests are flight vehicle preliminary design, multidisciplinary optimization, and aerostat design.

Ji Jinzu received his Ph.D. degree in the School of Aeronautic Science and Engineering at Beihang University in 2009. His research interests mainly include aircraft conceptual design and stealth.

Yu Dazhao received his Ph.D. degree at Naval Aeronautical and Astronautical University in 2007. His research interests mainly include aircraft security, finite element analysis, and fatigue life.